

Degenerate Quasicrystal of Hard Triangular Bipyramids

Amir Haji-Akbari,¹ Michael Engel,¹ and Sharon C. Glotzer^{1,2,*}

¹*Department of Chemical Engineering, University of Michigan, Ann Arbor, MI 48109*

²*Department of Materials Science and Engineering, University of Michigan, Ann Arbor, MI 48109*

(Dated: June 13, 2022)

We report a degenerate quasicrystal in Monte Carlo simulations of a collection of hard triangular bipyramids each comprising of two regular tetrahedra sharing a single face. The dodecagonal quasicrystal is similar to that recently reported for hard tetrahedra but degenerate in the pairing of tetrahedra, and self assembles at packing fractions above 54%. Free energy calculations show that a triclinic crystal, with the maximum packing fraction of 85.63%, is preferred at packing fractions above 79%.

Hard disks and spheres order into hexagonal and face-centered cubic crystals, respectively, above a certain packing fraction. A more complex phase behavior is observed if the disks or spheres are rigidly bonded into dimers (dumbbells) [1–4]. A solid phase, disordered in the orientation of dimers while ordered on the monomer level, forms if the distance between monomers within a dimer is roughly the diameter of a monomer. This equilibrium solid phase can be alternatively understood as a random pairing of neighboring monomers within the native monomer crystal. The resulting thermodynamic ensemble of ground states is degenerate and the structure is therefore called a degenerate crystal. As shown by Wojciechowski *et al.* [1] for hard disks, the entropy associated with the degeneracy exceeds the entropy from excluded volume effects, which by itself is sufficient to drive the crystallization of hard monomers. Other consequences of the pairing of monomers into dimers include topological defects [5], a restricted, glassy dislocation motion [6, 7], and unusual elastic properties [8].

Although degenerate crystals can potentially assemble from dimers of hard shapes other than disks and spheres, few examples have been reported. One reason is the competition between degenerate crystals and the liquid crystalline phases frequently observed for particles with large aspect ratios. For example, elongated tetragonal parallelepipeds, which for an aspect ratio of 2:1 can be viewed as dimers of face-sharing cubes, form a degenerate parquet phase at intermediate densities before transforming into a smectic liquid crystal that eventually crystallizes [9]. Another simple dimer is the triangular bipyramid (TBP), which consists of two face-sharing, regular tetrahedra (Fig. 1a). The TBP is the simplest face-transitive bipyramid and the twelfth of the 92 Johnson solids. The lack of inversion symmetry of the TBP, however, makes lattice packings non-optimal [10], and thus it is potentially more interesting as a dimer than other examples. Moreover, the recent synthesis of TBP-shaped nanoparticles and colloids [11–14] makes the investigation of this building block of practical relevance.

In both of the known ordered phases of hard, regular tetrahedra, each tetrahedron is in almost-perfect face-to-face contact with at least one other tetrahedron.

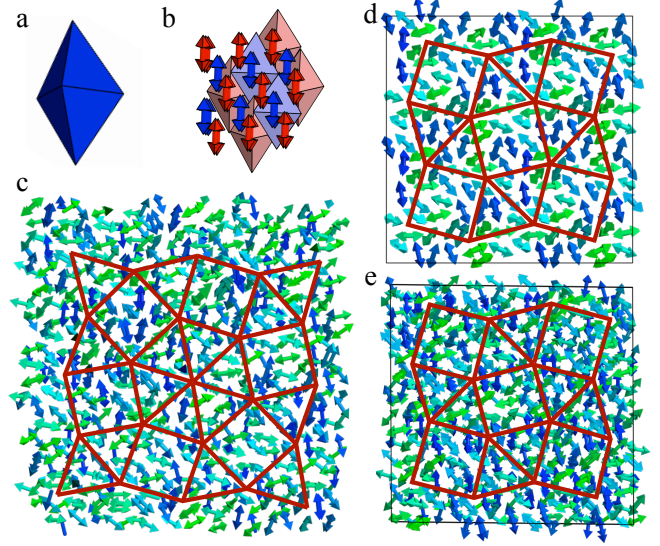


FIG. 1: Phases formed by (a) triangular bipyramids (TBPs): (b) TBP crystal, (c) degenerate quasicrystal, (d) regular quasicrystal approximant, (e) degenerate quasicrystal approximant. For visualization purposes, we show member tetrahedra of most TBPs at 30% actual size and connect their centers with bonds. In (c-e), tetrahedra and bonds are colored according to their orientation projected on the plane.

The densest known packing of tetrahedra ($\phi = \frac{4000}{4671} \approx 85.63\%$) is a parallel arrangement of two dimers (four tetrahedra) – that is, two TBPs – in a triclinic unit cell to form a dimer crystal [15, 16], which we refer to in the present paper as the TBP crystal. Degenerate phases are impossible in the TBP crystal because the contacts between the tetrahedra in different TBPs are highly imperfect [17]. At lower packing fractions, hard tetrahedra assemble into a dodecagonal quasicrystal [18], in which the tetrahedra form a decorated square-triangle tiling [19]. Unlike the TBP crystal, degenerate phases are possible in the quasicrystal due to the almost-perfect face-to-face contacts between all neighboring tetrahedra. Quasicrystals are solids with long-range order but without periodicity [20]. Originally discovered in metallic alloys [21], many alloy quasicrystals are now known, and a handful of quasicrystals have been reported in non-metallic sys-

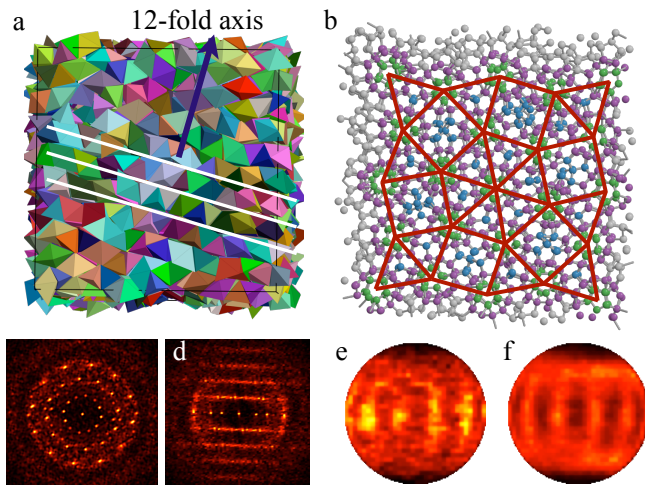


FIG. 2: (a) TBPs assemble into a dodecagonal quasicrystal in isobaric and isochoric Monte Carlo simulations. (b) The square-triangle tiling obtained by connecting the centers of 12-fold rings of member tetrahedra. (d,e) Diffraction patterns with centers of member tetrahedra as scatterers calculated (c) perpendicular to and (d) across the layers. (e) Intra-TBP and (f) total bond order diagrams.

tems. Among them are quasicrystals made from spherical micelles [22], binary nanoparticles [23], and hard tetrahedra [18].

In this Letter, we investigate the phase behavior of hard TBPs and report a degenerate quasicrystal. The notion of degeneracy should not be confused with the extensively studied degeneracy associated with random tiling quasicrystals [24, 25] where tiles with unique decoration patterns mix to form random tilings. We instead report a new type of randomness in the level of decorating individual tiles, in addition to the degeneracy of the random tiling.

We use isochoric and isobaric Monte Carlo (MC) simulations to study hard TBPs, which we model as perfect polyhedra with sharp vertices and edges of unit length σ . Simulations are carried out within periodic boxes with system sizes ranging from 432 to 8,000 particles. Each isochoric MC cycle comprises one update per particle on average, which is either a trial translation or a trial rotation with equal probabilities. An additional box trial move is included per isobaric cycle. For fluid phases, the box is resized isotropically only, while for crystals its shape is also allowed to fluctuate. Free energies are calculated using thermodynamic integration and a modified Frenkel-Ladd method [2, 26] as described in detail in [17]. Further details and simulation parameters are given in Ref. [29].

The dodecagonal quasicrystal of TBPs forms spontaneously from the equilibrium fluid phase at packing fractions above 54%. Fig. 2a depicts a side view of the quasicrystal formed in an isobaric simulation of 2,624 TBPs at reduced pressure $P^* = P\sigma^3/k_B T = 46$ and sub-

sequently compressed to a packing fraction of 81.34%. TBPs arrange into layers (white lines), which stack on top of each other perpendicular to the 12-fold symmetry axis (dark arrow). We confirmed that the formation of the quasicrystal occurs reproducibly in systems with at least a few thousand particles and does not depend on the shape of the simulation box.

The quasicrystal structure can be best understood by replacing each bipyramid by its two member tetrahedra. Fig. 2b depicts the centroids of tetrahedra within a few layers of Fig. 2a. Neighboring tetrahedra are connected with bonds [30]. Dodecagons that are depicted in purple in Fig. 2b correspond to rings of twelve member tetrahedra, a structural motif characteristic of the quasicrystal [18]. These rings are further capped with pentagonal dipyramids (PDs), five tetrahedra sharing an edge, visible in the figure as pentagons (green) within dodecagons. Additional member tetrahedra, referred to as interstitials, fill the space between the rings and are depicted in dark blue. Together, dodecagons and PDs form motifs whose centers are the vertices of square and triangle tiles. Their mixing gives the square-triangle tiling its overall twelve-fold symmetry as observed in the diffraction pattern depicted in Fig. 2c. Layering along the 12-fold axis can be seen in Fig. 2d. Overall, the arrangement of the member tetrahedra is identical to that reported in the hard tetrahedron system [18].

To elucidate how the bipyramids are arranged within the quasicrystal, we compare statistical distributions of intra-TBP bonds (bonds that connect member tetrahedra within TBPs) and the set of all bonds in the quasicrystal by projecting both sets onto the surface of a unit sphere. The resulting diagrams are referred to as intra-TBP and total bond order diagrams, respectively. We observe no significant distinction between these bond order diagrams (Figs. 2e,f). This suggests that the pairing of tetrahedra in the quasicrystal does not follow a pre-defined set of rules and is instead random. Motivated by studies of hard sphere dimers [1], we refer to the TBP quasicrystal as a degenerate quasicrystal (DQC). The randomness can be seen clearly in Fig. 1c. It is surprising that the structural quality of the DQC is uncompromised despite the additional geometrical constraints imposed on the system by pairing tetrahedra into TBPs. For instance, we find that the maximum packing fraction achieved by replacing the bipyramids with individual member tetrahedra and then compressing is statistically identical to that obtained in simulations of hard tetrahedra.

Approximants are periodic phases that are structurally similar to the quasicrystal locally [27]. Constructing an approximant of the TBP quasicrystal involves not only choosing a periodic tiling and decorating it with tetrahedra, but also pairing the tetrahedra into bipyramids. We choose the (3.4.3².4) Archimedean tiling which, in the case of hard tetrahedra, gives rise to the densest ap-

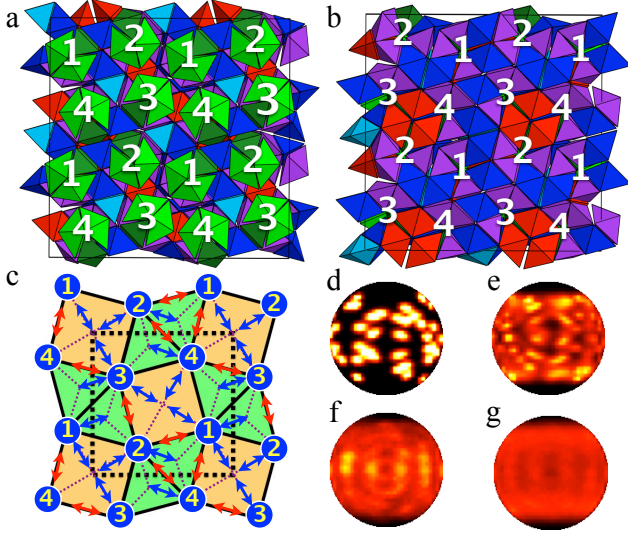


FIG. 3: (a) Top and (b) bottom views of the regular approximant. The unit cell has 41 triangular bipyramids. Particles are colored according to their environment: PD-PD (light green), PD-ring (dark green), intra-ring (purple), ring-ring (red), ring-interstitial (blue), interstitial-interstitial (cyan). (c) Schematics of the unit cell with connections between neighboring rings and between rings and central interstitials shown with red and blue double-arrows, respectively. (d,f) Intra-TBP and (e,g) total bond order diagrams for (d,e) the regular approximant at $\phi = 0.70$ and (f,g) the degenerate approximant at $\phi = 0.58$.

proximant [18]. There is no unique way of pairing tetrahedra into TBPs even within a single unit cell of the approximant due to degeneracies associated with rotations of the capping PDs. In particular, it is not possible to avoid breaking the four-fold symmetry of the approximant unit cell in the pairing process. We constructed a *regular approximant* by retaining as much of the symmetry as possible. Top and bottom views of the constructed approximant are depicted in Figs. 3a,b while a unit cell is depicted in Fig. 3c where ring-ring and ring-interstitial connections are highlighted. We find that the regular approximant can be compressed to a maximum packing fraction of 83.39%, a bit less than the maximum packing fraction of 85.03% achieved for the quasicrystal approximant constructed of individual tetrahedra [18]. The distinctive difference between the intra-TBP (Fig. 3d) and the total bond order diagrams (Fig. 3e) is a result of this deterministic pairing (Fig. 1d).

By expanding the regular approximant, we find that it melts at $P^* \leq 35$ and packing fractions $\phi < 54\%$. But before melting, the crystal slowly transforms into a more loosely packed structure in which tetrahedra are paired at random into TBPs, just as in the DQC, although their positions and orientations are unchanged (Fig. 1e). The resulting structure is therefore degenerate to the tetrahedron-based approximant and we refer to it as a degenerate approximant (DA). In contrast to the

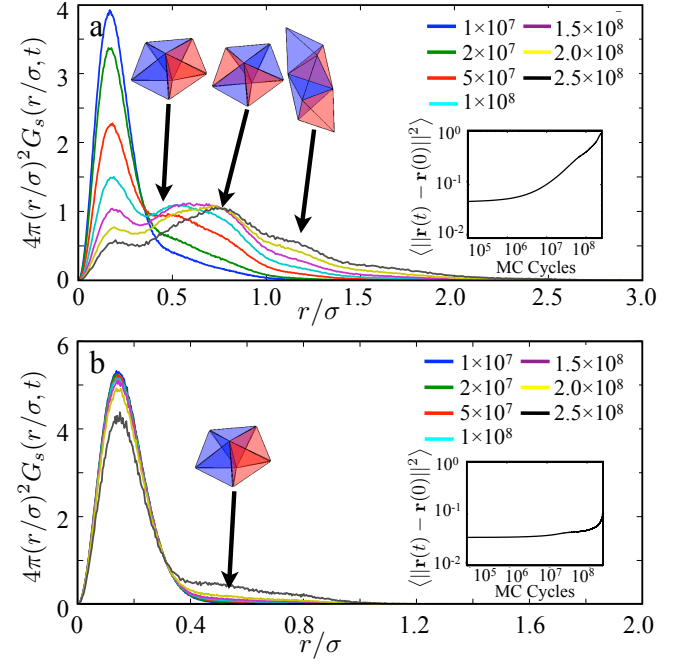


FIG. 4: The self part of the van Hove correlation function $G_s(r, t)$ measures the particle motion in the approximant. The separation distance $r(t)$ is calculated between centers of mass of member tetrahedra. (a) Large rearrangements occur at $\phi = 0.57$. (b) There is little motion present at $\phi = 0.60$.

regular approximant, the intra-TBP bond order diagram and the total bond order diagram of the DA are identical (Fig. 3f,g), which further confirms random pairing. We find that the transformation from regular to degenerate approximant is irreversible on the time scale of our simulations. Since the DA can only be recompressed to a density of 82.88%, which is lower than the maximum density of the regular approximant, the DA has to be stabilized by its pairing disorder close to melting.

To understand how the regular approximant transforms into the DA, we note (Fig. 2b) that the arrangement of the member tetrahedra can be alternatively understood as a spanning network of interpenetrating PDs [18]. In the hard tetrahedron system, PDs can easily rotate around their principal axes [17]. Such rotations are also essential in understanding the local rearrangements of bipyramids at densities below 60%. As shown in Fig. 4b, TBPs move very little at $\phi = 0.6$. Even after 250 million MC cycles only a small fraction of TBPs have moved as much as σ . A much faster dynamics occurs at $\phi = 0.57$. Particles at or near that density move over discrete distances that are characteristic of a PD network (Fig. 4a). These rearrangements change neither the tiling nor its decoration. Instead, they reshuffle the pairing pattern by a sequence of PD rotations. After a sufficiently large number of reshuffling moves the DA emerges from the regular approximant.

Next we study the relative thermodynamic stability

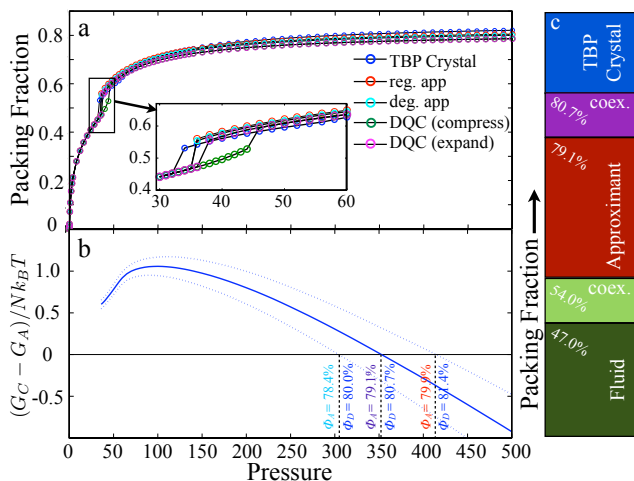


FIG. 5: (a) Equation of state for the TBP crystal, the degenerate quasicrystal, the regular and the degenerate approximants. (b) The free energy difference between the TBP crystal and the approximant. (c) Equilibrium phases of hard TBPs.

of various phases. We first compare the DQC and its approximant. Since they are locally identical, they are expected to have similar configurational entropies. The thermodynamic stability will thus be governed by packing fraction only. As observed in Fig. 5a, both the regular and the degenerate approximant are slightly denser than the DQC at all pressures. This suggests they may be thermodynamically preferred over the DQC. The observation that the approximant melts at lower pressures when expanded is a further indication that it is thermodynamically preferred. Nevertheless, the DQC remains the only ordered phase that forms in our simulations. It is also the only structure we expect to be observed in experiments of hard nanocolloidal TBPs since the kinetic process of transforming from the DQC into the approximant is extremely slow.

Next, we compare the approximant with the TBP crystal by calculating the free energy difference between them. As shown in Fig. 5b, the approximant has a lower free energy than the TBP crystal for packing fractions below 79%. A phase transition occurs at $P_c^* = 356 \pm 50$, corresponding to coexistence packing fractions of $\phi_{c,app} = (79.7 \pm 0.8)\%$ and $\phi_{c,TBP} = (80.7 \pm 0.7)\%$. The thermodynamic stability of the approximant at lower densities can be attributed to the additional configurational entropy associated with collective motions of particles. Such motions are not present in the TBP crystal. The phase diagram of the hard TBP system is depicted in Fig. 5c.

Remarkably, hard TBPs not only prefer a complex quasicrystal over the simpler TBP crystal at intermediate packing fractions, but also form it on timescales comparable to that previously observed in the hard tetrahedron system. This is surprising because, in comparison to tetrahedra, the motion of the highly anisotropic bipyra-

mids is considerably more constrained. Nevertheless, the degeneracy of the quasicrystal helps it form easily in simulation. Random pairing allows TBPs to join existing seeds of the DQC without forming configurations that are kinetically trapped due to incorrect pairing. Particle rearrangements needed for the formation and growth of the seed are also feasible due to the local similarity of the fluid and the quasicrystal [18, 28]. Finally, the degeneracy and the existence of ring-ring and ring-interstitial “cross-links” adds rigidity to the TBP structures. This means that the TBP system might be superior over the tetrahedron system in terms of its mechanical properties, just as for crystals of hard sphere dimers compared to crystals of their monomers [8].

In conclusion we have shown that hard triangular bipyramids form a degenerate dodecagonal quasicrystal. Our finding is only the second quasicrystal formed with hard particles, the first reported degenerate quasicrystal, and one of only a few quasicrystals formed in non-atomistic systems. Our results suggest that degenerate phases are not restricted to simple close-packed crystals and might be common in dimer systems.

This work was supported in part by the U. S. Air Force Office of Scientific Research (FA9550-06-1-0337) and by a U.S. Department of Defense National Security Science and Engineering Faculty Fellowship (N00244-09-1-0062). M.E. acknowledges support from the Deutsche Forschungsgemeinschaft. A.H-A acknowledges support from the University of Michigan Rackham Predoctoral Fellowship program.

* Electronic address: sglotzer@umich.edu

- [1] K. W. Wojciechowski, D. Frenkel, and A. C. Brańka, Phys. Rev. Lett. **66**, 3168 (1991).
- [2] C. Vega, E. P. A. Paras, and P. A. Monson, J. Chem. Phys. **96**, 9060 (1992).
- [3] A. P. Malanoski and P. A. Monson, J. Chem. Phys. **107**, 6899 (1997).
- [4] M. Marechal and M. Dijkstra, Phys. Rev. E **77**, 061405 (2008).
- [5] M. O. Blunt, J. C. Russel, M. del Carmen Jimenez-Lopez, J. P. Garrahan, X. Lin, M. Schroder, N. R. Champness, and P. H. Beton, Science **322**, 1077 (2008).
- [6] S. J. Gerbode, S. H. Lee, C. M. Liddell, and I. Cohen, Phys. Rev. Lett. **101**, 058302 (2008).
- [7] S. J. Gerbode, U. Agarwal, D. C. Ong, C. M. Liddell, F. Escobedo, and I. Cohen, Phys. Rev. Lett. **105**, 078301 (2010).
- [8] K. V. Tretyakov and K. W. Wojciechowski, J. Non-Cryst. Solids **352**, 4221 (2006).
- [9] B. S. John, C. Juhlin, and F. A. Escobedo, J. Chem. Phys. **128**, 044909 (2008).
- [10] S. Torquato and Y. Jiao, Nature **460**, 876 (2009).
- [11] B. J. Wiley, Y. Xiong, Z.-Y. Li, Y. Yin, and Y. Xia, Nano Letters **6**, 765 (2006).
- [12] X. Tang, M. Tsuji, M. Nishio, and P. Jiang, Bull. Chem.

- Soc. Jpn. **82**, 1304 (2009).
- [13] J. Zhang, S. Li, J. Wu, G. C. Schatz, and C. A. Mirkin, *Angew. Chem. Int. Ed.* **48**, 7787 (2009).
 - [14] J. Zhang, M. R. Langille, and C. A. Mirkin, *JACS* **132**, 12502 (2010).
 - [15] E. R. Chen, M. Engel, and S. C. Glotzer, *Disc. Comp. Geom.* **44**, 253 (2010).
 - [16] Y. Kallus, V. Elser, and S. Gravel, *Disc. Comp. Geom.* **44**, 245 (2010).
 - [17] A. Haji-Akbari, M. Engel, and S. Glotzer (2011), arXiv:1106.4765.
 - [18] A. Haji-Akbari, M. Engel, A. S. Keys, X. Y. Zheng, R. Petschek, P. Palfy-Muhoray, and S. C. Glotzer, *Nature* **462**, 773 (2009).
 - [19] M. Oxborrow and C. L. Henley, *Phys. Rev. B.* **48**, 6966 (1993).
 - [20] D. Levine and P. J. Steinhardt, *Phys. Rev. Lett.* **53**, 2477 (1984).
 - [21] D. Shechtman, I. Blech, D. Gratias, and J. W. Cahn, *Phys. Rev. Lett.* **53**, 1951 (1984).
 - [22] X. Zeng, G. Ungar, Y. Liu, V. Percec, S. Dulcey, and J. Hobbs, *Nature* **428**, 157 (2004).
 - [23] D. V. Talapin, E. V. Shevchenko, M. I. Bodnarchuk, X. Ye, J. Chen, and C. B. Murray, *Nature* **461**, 964 (2009).
 - [24] V. Elser, *Phys. Rev. Lett.* **54**, 1730 (1985).
 - [25] K. J. Strandburg, L.-H. Tang, and M. V. Jaric, *Phys. Rev. Lett.* **63**, 314 (1989).
 - [26] D. Frenkel and A. J. C. Ladd, *J. Chem. Phys.* **81**, 3188 (1984).
 - [27] A. I. Goldman and R. F. Kelton, *Rev. Mod. Phys.* **65**, 213 (1993).
 - [28] A. S. Keys and S. C. Glotzer, *Phys. Rev. Lett.* **99**, 235503 (2007).
 - [29] See supplementary material for more details.
 - [30] Two tetrahedra are defined as neighbors if their distance lies within the first peak of $g_t(r)$, the radial distribution function based on the centroids of the tetrahedra.

SUPPLEMENTARY INFORMATION

Free energy calculations

We use a modified version of the Frenkel-Ladd thermodynamic integration scheme [2, 26] to calculate the Helmholtz free energy differences between various crystals in the system. The Gibbs free energy is then determined from the Helmholtz free energy together with the equation of state. The equation of state is also used to extrapolate the Gibbs free energies to pressures where no Frenkel-Ladd calculation can be performed by integrating $dG = VdP$. The values of γ_{\max} and c chosen in this study are included in Table I. Further technical of the free energy calculation scheme can be found in [17], where the same method was applied to a system of hard tetrahedra.

Van Hove correlation function and structure factor

The van Hove correlation function and the structure factor are calculated for centroids of member tetrahedra in the hard TBP quasicrystal approximant. To determine the structure factor, the centroids are convoluted with a Gaussian and projected along the observation direction. The resulting pattern is sheared into a square, discretized, fast Fourier transformed, and then sheared back.

Dense packings

The densest unit cells of the TBP crystal and the regular approximant are given in Tables II and III, respectively. In the tables, the orientation of each TBP is represented by a unit quaternion $\mathbf{q} = (q_t, q_x, q_y, q_z)$ with

rotation matrix

$$\begin{pmatrix} q_t^2 + q_x^2 - q_y^2 - q_z^2 & 2(q_x q_y - q_t q_z) & 2(q_x q_z + q_t q_y) \\ 2(q_x q_y + q_t q_z) & q_t^2 - q_x^2 + q_y^2 - q_z^2 & 2(q_y q_z - q_t q_x) \\ 2(q_x q_z - q_t q_y) & 2(q_y q_z + q_t q_x) & q_t^2 - q_x^2 - q_y^2 + q_z^2 \end{pmatrix}$$

The vertices of the TBP with $\mathbf{q} = (1, 0, 0, 0)$ are given by:

$$\begin{aligned} \mathbf{v}_{1,2} &= \left(0, 0, \pm \frac{4\sqrt{3}}{3}\right), \mathbf{v}_{3,4} = \left(-\frac{\sqrt{6}}{3}, \pm\sqrt{2}, 0\right), \\ \mathbf{v}_5 &= \left(\frac{2\sqrt{6}}{3}, 0, 0\right). \end{aligned}$$

TABLE I: Simulation details for the calculation of the equation of state (EOS), quasicrystal (QC) assembly, and thermodynamic integration. Several independent runs were performed for each state point to assure accurate statistics.

Phase	Objective	Ensemble	System size	MC sweeps	Parameters
Fluid	EOS calculation	isobaric	2,624	10^7	$0.01 \leq P^* \leq 60$
Fluid	QC assembly	isobaric	1,458 – 2,624	10^8	$40 \leq P^* \leq 60$
Fluid	QC assembly	isochoric	8,000	10^8	$0.5 \leq \phi \leq 0.6$
TBP crystal	EOS calculation	isobaric	432	10^7	$32 \leq P^* \leq 10,000$
Quasicrystal	EOS calculation	isobaric	2,624	10^7	$36 \leq P^* \leq 10,000$
Approximant	EOS calculation	isobaric	656	10^8	$35 \leq P^* \leq 10,000$
Approximant	Dynamics	isochoric	656	3×10^8	$0.57 \leq \phi \leq 0.80$
TBP crystal	Therm. Integration	isochoric	432	2×10^5 per γ	$0 \leq \gamma \leq 5 \times 10^5, c = 4$ $0.70 \leq \phi \leq 0.80$
Approximant	Therm. Integration	isochoric	656	2×10^5 per γ	$0 \leq \gamma \leq 5 \times 10^5, c = 4$ $0.60 \leq \phi \leq 0.80$

TABLE II: A unit cell of the TBP crystal with $\phi = 85.6347\%$. The lattice vectors are given by $b_1 = (8/5, 12/5, 4/5)$, $b_2 = (3/8, 97/80, 191/80)$, $b_3 = (12/5, 3/20, 3/2)$. The positions and quaternions of the two particles in the unit cell are given.

i	x_i	y_i	z_i	$q_{t,i}$	$q_{x,i}$	$q_{y,i}$	$q_{z,i}$
1	0	0	0	0.880476	-0.364705	0.279848	-0.115917
2	-26/15	-79/120	-1/120	-0.279848	0.115917	0.880476	-0.364705

TABLE III: A unit cell of the regular approximant with $\phi = 83.39\%$. Lattice vectors are given by $b_1 = (9.968511, 0, 0)$, $b_2 = (0, 10.127064, 0)$, $b_3 = (0, 0, 2.597388)$. There are 41 particles in the unit cell; their positions and orientations are given.

i	x_i	y_i	z_i	$q_{t,i}$	$q_{x,i}$	$q_{y,i}$	$q_{z,i}$
1	2.577563	2.034764	0.468262	-0.571639	-0.070079	0.373327	0.727286
2	4.166214	-1.756756	0.615969	0.857393	0.268822	-0.248715	-0.361598
3	-3.084856	-2.367062	0.416958	0.724350	0.367424	0.073032	0.578776
4	-4.695950	1.275885	0.604617	0.360239	0.252360	0.269435	0.856707
5	-4.116796	-0.891580	0.416929	0.432066	-0.509884	0.631452	0.393199
6	3.525531	0.477749	0.416545	0.351928	0.669668	0.463299	-0.461567
7	4.713508	-0.238356	-0.535056	0.079851	-0.418922	-0.567332	0.704460
8	4.456554	-2.994345	-0.340993	0.780466	0.401093	-0.425661	0.220927
9	-3.924608	-3.468885	-0.349299	-0.3170322	0.435670	0.725220	0.428647
10	4.827924	-4.702429	-0.156272	-0.126458	0.202731	0.414845	0.877959
11	3.991628	3.708089	0.056029	0.183353	0.789651	0.086049	-0.579162
12	3.568246	-4.595877	-1.080604	0.753728	-0.607784	-0.001876	0.249979
13	-3.745622	5.05501	-1.100613	0.781173	-0.449416	0.429698	-0.056161
14	4.196450	2.277453	-0.597993	-0.359044	0.680617	0.267072	-0.580104
15	2.386453	4.616089	-0.644698	0.236756	-0.425760	0.711068	-0.507009
16	1.938061	-3.806682	-0.664818	-0.348159	-0.057568	0.878425	0.322244
17	0.917585	-4.718172	1.159099	-0.342416	-0.075558	-0.566189	0.745970
18	-0.058226	4.024636	-0.779047	-0.218536	0.292761	0.406125	0.837613
19	-0.015417	1.965532	-0.686062	-0.575956	0.092427	0.547770	0.599733
20	-2.649724	4.204716	-0.354660	0.507751	-0.424226	0.583457	0.470956
21	-1.458027	4.257144	1.193589	0.729663	-0.577430	0.065861	0.360318
22	-1.775258	2.638762	-0.711381	0.665486	0.459141	-0.016513	0.588256
23	-0.462803	-4.240967	-0.781489	0.852972	0.387175	-0.303437	0.174526
24	-4.267006	3.386144	-0.468613	-0.000176	0.782728	0.478271	0.398237
25	0.590989	-2.637448	-0.391425	0.687108	-0.072288	0.705971	0.155766
26	0.931505	0.557550	0.042641	0.541333	-0.498375	0.611842	0.290223
27	-0.327549	-1.570523	-1.103805	0.132441	-0.297442	-0.551238	0.768196
28	-1.197224	1.002383	-1.098048	0.472711	-0.577011	-0.124144	0.654362
29	-2.669607	-0.000869	-0.332883	-0.555831	-0.432230	0.706413	-0.072178
30	1.360992	-1.043831	-0.494023	-0.218324	0.282330	0.279283	0.891418
31	-2.068599	-1.475994	-0.432188	0.177372	0.552632	0.095644	0.808696
32	-0.824950	-0.279502	-0.173665	0.812864	0.301838	-0.360459	-0.343825
33	1.875960	3.734302	0.688700	0.637200	0.525578	0.372843	0.422766
34	0.851339	2.543637	0.651610	-0.136354	-0.216962	0.718646	0.646438
35	2.521194	-1.370751	0.914745	0.340997	0.338882	0.555950	0.678086
36	2.668774	-2.952467	0.793322	0.397482	0.528194	-0.528780	-0.532363
37	-2.319993	-4.114732	0.661033	-0.409719	-0.392437	0.521386	0.637400
38	-1.344552	-2.862699	0.634106	0.637069	0.725629	0.218256	0.141312
39	-2.939764	1.003839	0.920083	0.691960	0.5626407	-0.313482	-0.326121
40	-3.430922	2.530387	0.770143	0.488982	0.502086	0.569902	0.428972
41	2.380887	0.537208	-0.641148	-0.668029	0.708420	-0.035948	-0.224914